CHEMISTRY OF MATERIALS

Article

pubs.acs.org/cm

Molecular Engineering of Nonhalogenated Solution-Processable Bithiazole-Based Electron-Transport Polymeric Semiconductors

Boyi Fu,[†] Cheng-Yin Wang,[‡] Bradley D. Rose,[§] Yundi Jiang,[†] Mincheol Chang,[†] Ping-Hsun Chu,[†] Zhibo Yuan,[∥] Canek Fuentes-Hernandez,[‡] Bernard Kippelen,[‡] Jean-Luc Brédas,[§] David M. Collard,[∥] and Elsa Reichmanis*[,†,∥,⊥]

[†]School of Chemical & Biomolecular Engineering, Georgia Institute of Technology, 311 Ferst Drive, Atlanta, Georgia 30332-0100, United States

[‡]School of Electrical and Computer Engineering, Georgia Institute of Technology, 777 Atlantic Drive NW, Atlanta, Georgia 30332-0250, United States

[§]Solar and Photovoltaics Engineering Research Center, King Abdullah University of Science and Technology, Thuwal 23955-6900, Kingdom of Saudi Arabia

[∥]School of Chemistry & Biochemistry, Georgia Institute of Technology, 901 Atlantic Drive, Atlanta, Georgia 30332-0400, United States

[⊥]School of Materials Science and Engineering, Georgia Institute of Technology, 771 Ferst Drive, Atlanta, Georgia 30332-0245, United States

Supporting Information

ABSTRACT: The electron deficiency and trans-planar conformation of bithiazole is potentially beneficial for the electron-transport performance of organic semiconductors. However, the incorporation of bithiazole into polymers through a facile synthetic strategy remains a challenge. Herein, 2,2′-bithiazole was synthesized in one step and copolymerized with dithienyldiketopyrrolopyrrole to afford poly(dithienyldiketopyrrolopyrrole-bithiazole), **PDBTz**. **PDBTz** exhibited electron mobility reaching 0.3 $cm^2\ V^{-1}\ s^{-1}$ in organic field-effect transistor (OFET) configuration; this contrasts with a recently discussed isoelectronic conjugated polymer comprising an electron-rich bithiophene and dithienyldiketopyrrolopyrrole, which displays merely hole-transport characteristics. This inversion of charge-carrier transport characteristics confirms the significant potential for bithiazole in the development of electron-transport semiconducting materials. Branched 5-decylheptacyl side chains were incorporated into **PDBTz** to enhance polymer solubility, particularly in nonhalogenated, more environmentally compatible solvents. **PDBTz** cast from a range of nonhalogenated solvents exhibited film morphologies and field-effect electron mobility similar to those cast from halogenated solvents.

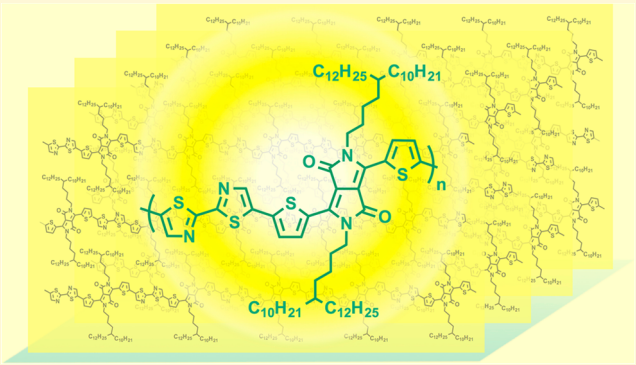

1. INTRODUCTION

The development of high-efficiency, air-stable electron-transport polymeric semiconductors for organic electronic devices has attracted much attention because of their importance in the fabrication of organic p−n junction devices, such as complementary metal-oxide-semiconductor (CMOS)-like logic circuits,[1,2] thermoelectrics,[3] heterojunction photovoltaics,[4−6] and organic light-emitting diodes.[7,8] For example, a combination of hole-transport and electron-transport semiconductors with comparable mobility values is required to implement CMOS-like logic, which is widely used in digital integrated circuits including microprocessors, microcontrollers, and static random access memory devices.[1,9,10] Significant advances in the development of hole-transport polymeric semiconductors have led to materials that demonstrate field-effect hole mobilities of up to 20 $cm^2\ V^{-1}\ s^{-1}$.[11,12] However, less progress has been made toward the development of electron-transport counterparts.[13−16] The more limited advances in this instance result from challenges associated with the stabilization and delocalization of the lowest unoccupied molecular orbital (LUMO) of π-conjugated polymers.[7,13,17,18] Stabilization of the LUMO means raising the electron affinity, which can be realized by materials that consist of electron-deficient conjugated repeat units.[13,18−20] The LUMO delocalization can be enhanced by backbone planarization and interchain stacking.[21]

Received: January 14, 2015
Revised: March 31, 2015
Published: April 1, 2015

DOI: 10.1021/acs.chemmater.5b00173
Chem. Mater. 2015, 27, 2928−2937

Scheme 1. Synthetic Route to Prepare PDBTz; Inset Image (bottom right) Shows a PDBTz Solution in *o*-Dichlorobenzene (DCB) and Spin-Coated Film of PDBTz from DCB (5 mg mL^{-1}) on a Glass Substrate

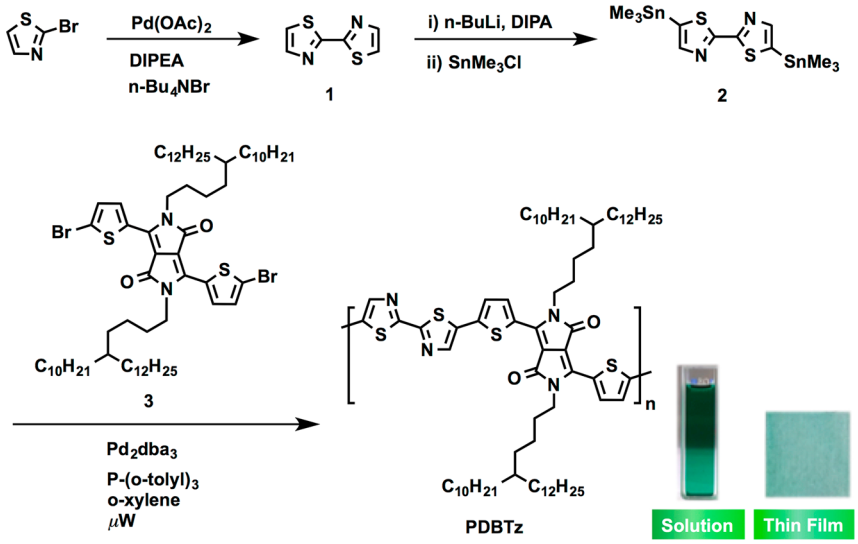

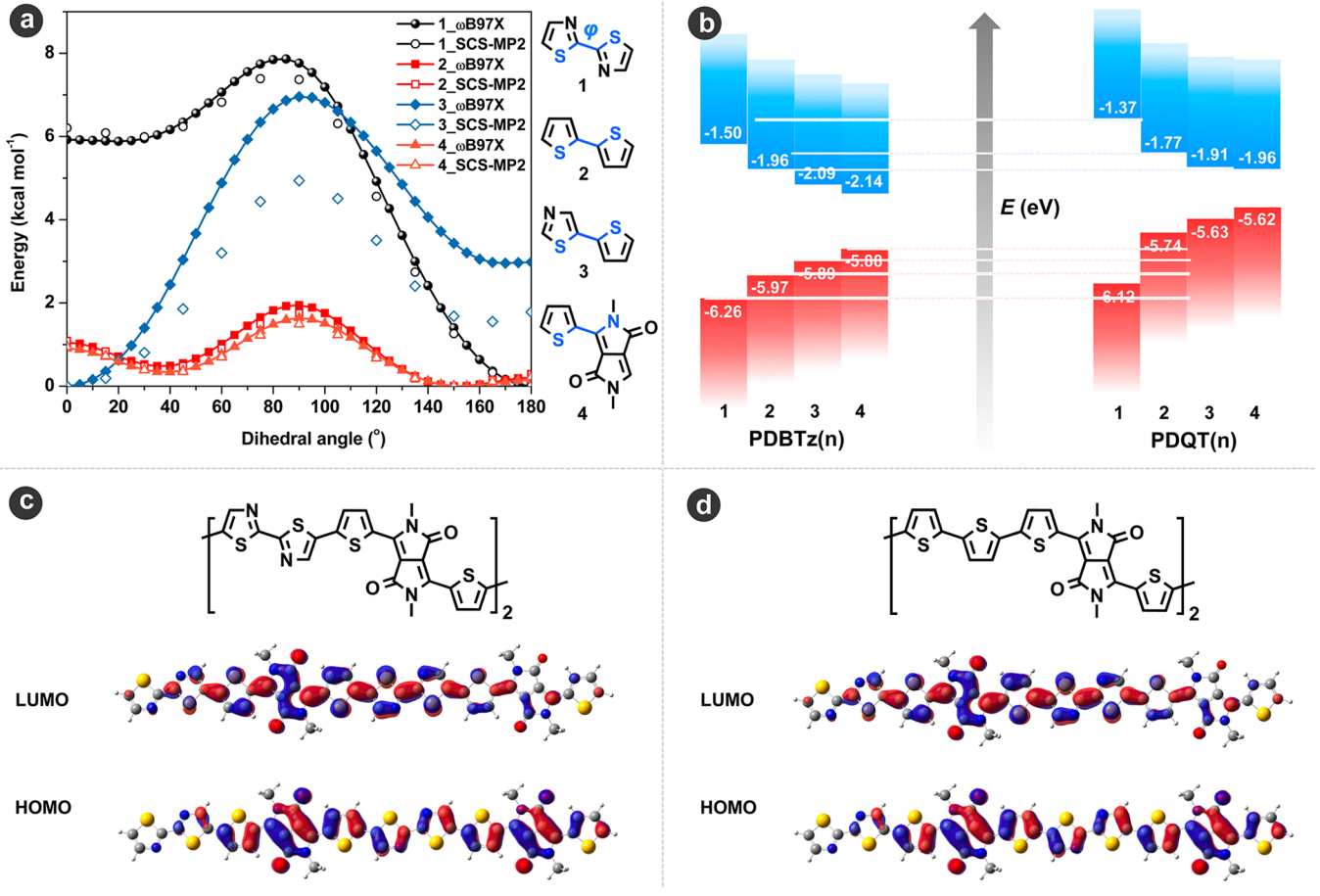

Figure 1. (a) DFT (tuned-ωB97X) and SCS-MP2 torsional energies of PDBTz subunits at different dihedral angles; dihedral angles (φ) for the subunits are highlighted in blue. (b) DFT HOMOs and LUMOs of the monomer (n = 1), dimer (n = 2), trimer (n = 3), and tetramer (n = 4) of PDBTz and PDQT. Illustrations of the DFT frontier molecular orbitals for the dimers of (c) PDBTz and (d) PDQT.

The 2,2′-bithiazole unit exhibits a number of features that could be attractive in the search for electron-transport conjugated polymers. The presence of electronegative nitrogen atoms lowers the LUMO energy in comparison to analogs that consist of electron-rich units such as thienyl derivatives.[22−26] The trans conformation of bithiazole (with a dihedral angle between the thiazole rings close to 180°, as confirmed by density functional theory, DFT, in this study, vide infra) can promote polymer backbone planarity, which extends intrachain π-conjugation and interchain $\pi-\pi$ stacking, in comparison to

DOI: 10.1021/acs.chemmater.5b00173
Chem. Mater. 2015, 27, 2928−2937

Table 1. Hansen Solubility Parameters (δ_d, δ_p, and δ_h); Boiling Points (b.p.) for PDBTz, Dichlorobenzene (DCB), *o*-Xylene, *p*-Xylene, and Tetrahydronaphthalene (THN); and Hansen Solubility Parameter Spaces (R_a) and Solubilities of PDBTz in Each Solvent

	δ_d[a] (MPa$^{1/2}$)	δ_p[b] (MPa$^{1/2}$)	δ_h[c] (MPa$^{1/2}$)	R_a[d] (MPa$^{1/2}$)	solubility[e] (mg mL^{-1})	bp (°C)
PDBTz	20.0	1.2	5.1			n/a
DCB	19.2	6.3	3.3	5.64	7	180
o-xylene	17.8	1.0	3.1	4.84	7	144
p-xylene	17.6	1.0	3.1	5.20	5	138
THN	19.6	2.0	2.9	2.47	9	207

[a]δ_d: dispersion force solubility. [b]δ_p: dipolar intermolecular force solubility. [c]δ_h: hydrogen bonding solubility. [d]R_a: (HSP difference between PDBTz and solvents) calculated by eq 1. [e]PDBTz solubility in solvent at 90 °C.

analogs such as biphenyl that is not coplanar.[27−29] Thiazole has a large dipole moment of 1.6 D;[30,31] an antiparallel alignment between the two thiazole moieties within bithiazole leads to a net zero dipole, which is one driving force for planarization of bithiazole. Additionally, the large dipole of the thiazole unit could impart strong dipole−dipole interactions between bithiazole-based polymer chains.[32]

The bithiazole unit has been primarily used to build hole-transport donor−acceptor π-conjugated copolymers; bithiazole was considered as a weak acceptor. Recent studies indicated the feasibility of using bithiazole in developing electron-transport small molecular semiconductors;[32,33] and in a few cases, bithiazole-based polymers exhibited ambipolar properties.[34] Hence, the development of electron-transport polymeric semiconductors based on bithiazole could be envisioned, though no study has been reported as of yet. One significant challenge lies in the development of an efficient synthetic pathway to incorporate bithiazole units into π-conjugated molecules and polymers.[24,32] Herein, 2,2′-bithiazole was synthesized in one step, and copolymerized with a second electron-deficient monomer, dithienyl diketopyrrolopyrrole (TDPP), to afford the first example of a bithiazole-based electron-transport polymer, poly(dithienyldiketopyrrolopyrrole-bithiazole), **PDBTz**, as shown in Scheme 1. An isoelectronic conjugated polymer consisting of alternating electron-rich 2,2′-bithiophene units and TDPP (PDQT, see structure shown in Figure 1) exhibits pure hole-transport behavior.[35−37] Through comparison of **PDBTz** with PDQT, we set out to explore the capability of bithiazole on tailoring hole and electron-transport characteristics, with the expectation that the bithiazole analog would enhance electron-transport behavior.

Side chain substitution on the bithiazole and dithienyl groups was avoided to minimize steric effects within the **PDBTz** backbone. Branched 5-decylheptadecyl (5-DH) side chains were utilized as they had been shown in our previous study to facilitate both polymer solubility and effective $\pi-\pi$ interchain interactions by virtue of having a branch point remote from the polymeric main chain.[38] Such a side chain was incorporated into the TDPP unit to promote $\pi-\pi$ interchain interactions and solubility in a wide range of solvents including non-halogenated options such as xylenes or 1,2,3,4-tetrahydronaphthalene (THN), which are more eco-friendly than halogenated alternatives.

Current semiconducting polymer solution processes for organic electronic devices primarily depend on the use of halogenated solvents such as chlorobenzene, *o*-dichlorobenzene (DCB), or 1,2,4-trichlorobenzene (TCB), which present significant health and environmental challenges and severely limit their future application. Thus, materials that can be processed from nonhalogenated media are highly desirable.[39−42] However, few such examples have been reported, and electron-transport polymeric semiconductors processable from nonhalogenated solvents are especially rare.[9] Here, **PDBTz** thin-film OFETs fabricated using nonhalogenated *o*-xylene, *p*-xylene, and THN, as well as DCB, were investigated. This allowed for a systematic study of solvent on semiconducting polymer thin-film ordering, texture, charge-carrier transport performance, and the practicality of developing high-mobility n-channel OFET devices via more environmentally benign processing.

2. RESULTS

2.1. Polymer Synthesis, Solubility, and Thermal Properties. The synthesis of **PDBTz** is outlined in Scheme 1, and complete synthetic details are provided in the Supporting Information. Commercially available 2-bromothiazole was homocoupled to afford 2,2′-bithiazole, **1**.[43] Metalation of **1** afforded distannane monomer **2**.[25] Conversion of **1** to **2** approached 100% on the basis of ^{1}H NMR analysis. However, **2** has limited stability: demetalation of 25−30 mol % of **2** back to **1** takes place within 1 week (Figure S6 in the Supporting Information). Hence, the polymerization should be carried out with freshly prepared monomer. **PDBTz** was prepared by Stille step-growth polymerization of monomer **2** with 3,6-bis(5-bromo-2-thienyl)-*N*,*N*-di(5-decylheptadecyl)diketopyrrolopyrrole monomer (**3**)[38] under microwave irradiation (160 °C for 2 h). The crude polymer was purified through precipitation from methanol followed by Soxhlet extraction to afford **PDBTz** that was further characterized. Gel permeation chromatography (GPC; 135 °C with TCB as eluent) indicated a number-average molecular weight (M_n) of 64 kg mol^{-1}, which corresponds to a degree of polymerization (DP) of 53, as shown in Table 2. The relatively large PDI of 3.6 is likely due to the polymer aggregation in solution.

The attainment of relatively high molecular weight material suggested that the resulting polymer has good solubility in *o*-xylene. Process solvents have a significant influence on the molecular ordering, morphology, and charge-carrier mobility of thin-film polymeric semiconductors. Hence, the characterization and processing of **PDBTz** in *o*-xylene along with two other similar nonhalogenated solvents, *p*-xylene and THN, were explored. The theoretical solubility of **PDBTz** was estimated using the Hansen solubility parameter space (R_a),[39,44] which describes the difference in Hansen solubility parameters (HSPs) of **PDBTz** (1) and solvents (2), as shown in eq 1

$$R_a = \sqrt{4(\delta_{d1} - \delta_{d2})^2 + (\delta_{p1} - \delta_{p2})^2 + (\delta_{h1} - \delta_{h2})^2} \quad (1)$$

DOI: 10.1021/acs.chemmater.5b00173
Chem. Mater. 2015, 27, 2928−2937

Table 2. PDBTz Molecular Weight, Photophysical, And Thermal Properties

				absorption maximum (eV)					
polymer	Mn (kD)]	PDI	DP	solution	film	E_g^{opt} (eV)	T_d^a (°C)	T_h^b (°C)	T_c^c (°C)
PDBTz	64	3.6	53	1.62, 1.77, 2.78, 3.82	1.62, 1.78, 2.77, 3.80	1.33	417	−44	−47

[a]T_d: decomposition temperature, defined as the temperature in which the polymer undergoes 5 wt % weight loss. [b]T_h: phase transition temperature upon heating process. [c]T_c: phase transition temperature upon cooling process.

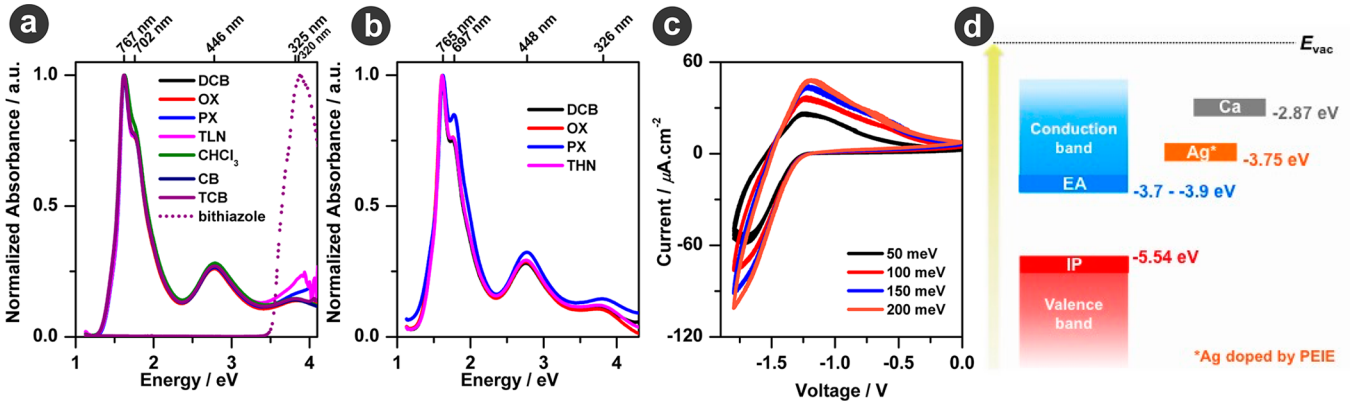

Figure 2. Photophysical and electrochemical properties of **PDBTz**: (a) UV/vis absorption spectra of **PDBTz** in solution (1×10^{-6} M; DCB, *o*-dichlorobenzene; OX, *o*-xylene; PX, *p*-xylene; THN, tetrahydronapthalene; $CHCl_3$, chloroform; CB, chlorobenzene; TCB, 1,2,4-trichlorobenzene); (b) UV/vis absorption spectra of **PDBTz** thin-films; (c) cyclic voltammograms of a drop-cast film of **PDBTz** on a platinum electrode (in 0.5 M Bu_4NPF_6/acetonitrile) at scan rates between 20 mV s^{-1} and 200 mV s^{-1} (five cycles at each scan rate); (d) ionization potential (IP) and electron affinity (EA) of **PDBTz** and workfunctions of Ca- and PEIE-doped Ag.

Table 3. PDBTz Ionization Potential and Electron Affinity

	UPS			DPV		CV	
polymer	IP[a] (eV)	ϕ (eV)	EA[b] (eV)	E_{red}^c (V)	EA (eV)	E_{red}^c (V)	EA (eV)
PDBTz	5.54	4.90	−3.7 - −3.9	−1.18	−3.90[d]	−1.30	−3.75[d]

[a]IP: ionization potential. [b]EA: electron affinity, taking into account an optical gap of ca. 1.33 eV and an exciton binding energy in the range of 0.3−0.5 eV. [c]E_{red}: reduction potential; [d]Calculated from onsets for reduction versus Fc/Fc+ (−5.08 eV versus vacuum[48,49]) + 5.08 eV.

where δ_d, δ_p, and δ_h refer to the dispersion force solubility parameter, dipolar intermolecular force solubility parameter, and hydrogen bonding solubility parameter, respectively. Lower values of R_a predict a lower cohesive energy density difference between **PDBTz** and a solvent, which corresponds to a weaker thermodynamic driving force for phase separation of solute from solvent and a higher solubility of the polymer.[45] The pertinent physical properties of **PDBTz** and the four solvents (DCB, *o*-xylene, *p*-xylene, and THN) are listed in Table 1 (the experimental and calculation details are provided in the Supporting Information). Solutions of **PDBTz** in the two xylenes exhibit similar R_a values as for **PDBTz** in DCB, whereas the corresponding value for THN is much lower. These results suggest similar or even better **PDBTz** solubility in the nonhalogenated solvents than in DCB. Experimental results indicate that **PDBTz** possesses solubility in the range of 5−9 mg mL^{-1} in the four solvents at 90 °C. **PDBTz** exhibits the lowest solubility in *p*-xylene (5 mg mL^{-1}), whereas the solubility is highest with THN (9 mg mL^{-1}).

PDBTz is stable up to 417 °C (see TGA characterization, Table 2 and Figure S7 in the Supporting Information), indicating high thermal stability. The polymer exhibits one endothermic (T_h = −44 °C) and one exothermic transition (T_c = −47 °C) upon heating and cooling, respectively (see DSC characterization, Table 2 and Figure S7 in the Supporting Information). In light of prior results using the same substituent, this most likely corresponds to the disordering and reordering processes associated with the 5-DH side chains.[38]

2.2. Photophysical Properties. The spectroscopic features of **PDBTz** solutions in the different solvents are quite similar. Peaks are observed at ca. 325, 446, 702, and 767 nm in the spectra of **PDBTz** in each solvent, as shown in Figure 2a. The bands with λ_{max} at ca. 446, 702, and 767 nm may be ascribed to TDPP units since solutions of the analogous diketopyrrolopyrrole-oligothiophene polymers exhibit similar features;[11,35−37] whereas the **PDBTz** band at λ_{max} of 325 nm was assigned to the bithiazole units, given that 2,2′-bithiazole (compound **1**) in THF exhibits an absorption band with λ_{max} at 320 nm (Figure 2a). The absorption spectra of **PDBTz** thin-films (Figure 2b) are essentially identical to those of the solution spectra, suggesting a similar rigid polymer chain conformation in the solid state as in solution. These results also suggest the self-assembly of **PDBTz** polymer chains in solution. Taking account of low **PDBTz** concentration in solution (1×10^{-6} M in Figure 2a), **PDBTz** has strong interchain interactions. On the basis of the absorption onset, the optical band gap (E_g^{opt}) of **PDBTz** is estimated as 1.33 eV. The increase in the intensity of the peak at 697 nm relative to that at 765 nm for the film (Figure 2b) in comparison to the solution (Figure 2a) suggests that **PDBTz** favors the interchain excitonic coupling[46,47] in thin films. **PDBTz** films cast from solutions in DCB, *o*-xylene, *p*-xylene, and THN exhibit similar spectroscopic characteristics, which indicates similar thin-film microstructure

DOI: 10.1021/acs.chemmater.5b00173
Chem. Mater. 2015, 27, 2928−2937

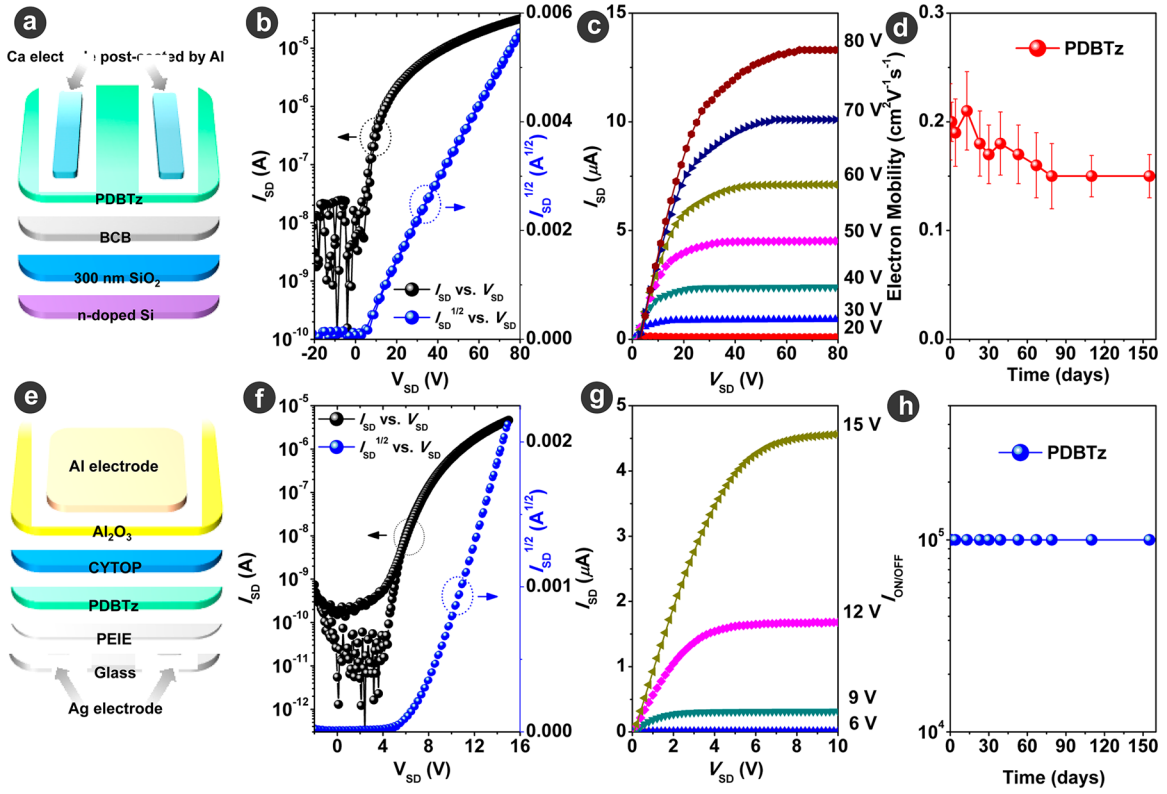

Figure 3. *I*–*V* curves for PDBTz-based OFETs with (a) bottom-gate/top-contact and (e) top-gate/bottom-contact architectures, and their corresponding (b, f) transfer and (c, g) output plots; effect of OFET stability under ambient conditions (25 °C and 55–60%RH) on (d) electron mobility and (h) $I_{ON/OFF}$.

Table 4. Electron Transport Properties of PDBTz Fabricated on Top-Contact/Bottom-Gate and Bottom-Contact/Top-Gate OFETs[a]

	TCBG				BCTG			
	μ_{eFET} ($cm^2\ V^{-1}\ s^{-1}$)				μ_{eFET} ($cm^2\ V^{-1}\ s^{-1}$)			
solvent	avg.	max	$I_{ON/OFF}$	V_{th} (V)	avg	max	$I_{ON/OFF}$	V_{th} (V)
DCB	0.17 (± 0.05)	0.26	1×10^5	5.5 (± 1.2)	0.17 (± 0.04)	0.21	1×10^5	7.8 (± 0.4)
o-xylene	0.14 (± 0.04)	0.18	1×10^5	8.0 (± 1.2)	0.08	0.08	1×10^4	0.8
p-xylene	0.24 (± 0.06)	0.31	1×10^5	4.0 (± 1.0)	0.08 (± 0.002)	0.08	1×10^3	0.8 (± 0.3)
THN	0.18 (± 0.07)	0.30	1×10^5	6.0 (± 3.5)	0.09 (± 0.007)	0.11	1×10^3	0.1 (± 0.1)

[a]BGTC characterization results were based on 5–8 of devices for each fabrication conduction; TGBC characterization results were 3–6 of devices for each fabrication conduction. These OFET devices were thermally annealed at 150 °C for 30 min.

(ordering and orientation) for all of the systems, although the film prepared using *p*-xylene is likely to form a stronger interchain excitonic coupling.

2.3. Characterization of Electronic Structure. The redox potentials of **PDBTz** thin-films were investigated using cyclic voltammetry (CV) and differential pulse voltammetry (DPV) (Figure S9 in the Supporting Information). **PDBTz** exhibits an onset for reduction at −1.30 V versus Fc/Fc^+ (−5.08 eV versus vacuum[48,49]) by CV, and −1.18 V (versus Fc/Fc^+) by DPV, as shown in Table 3, which corresponds to an electron affinity of −3.8 to −3.9 eV. The reversibility of the reduction, as shown in Figure 2c, demonstrates the stability of reduced **PDBTz** as an electron carrier. However, **PDBTz** exhibits an irreversible electrochemical oxidation process as demonstrated by both CV and DPV, with a peak onset at +0.82 V (versus Fc/Fc^+) by CV and +0.66 V (versus Fc/Fc^+) by DPV (Figure S9b in the Supporting Information). These electrochemical results are opposed to the typical hole-transport polymeric semiconductors that have a reversible oxidation with no obvious reduction.[20,35,38]

Thin films of **PDBTz** were characterized by ultraviolet photoelectron spectroscopy (UPS) to determine the intrinsic ionization potential (IP) and work function (φ) (Table 3 and Figure S10 in the Supporting Information). The 5.54 eV **PDBTz** ionization potential suggests good ambient stability toward oxidation.[18] Taking into account an optical gap of ca. 1.33 eV and an exciton binding energy in the range of 0.3–0.5 eV[50] would lead to an electron affinity on the order of −3.7 to −3.9 eV, which is consistent with the CV/DPV estimate. Such an electron affinity implies a good ambient stability for electron-transport organic semiconductors.[7,13]

2.4. Field-Effect Electron Transport. **PDBTz** charge-carrier transport properties were studied using organic field-effect transistors (OFETs) with top-contact/bottom-gate (TCBG) and bottom-contact/top-gate (BCTG) architectures, as shown in Figure 3. With the aim of minimizing barriers to

DOI: 10.1021/acs.chemmater.5b00173
Chem. Mater. 2015, 27, 2928–2937

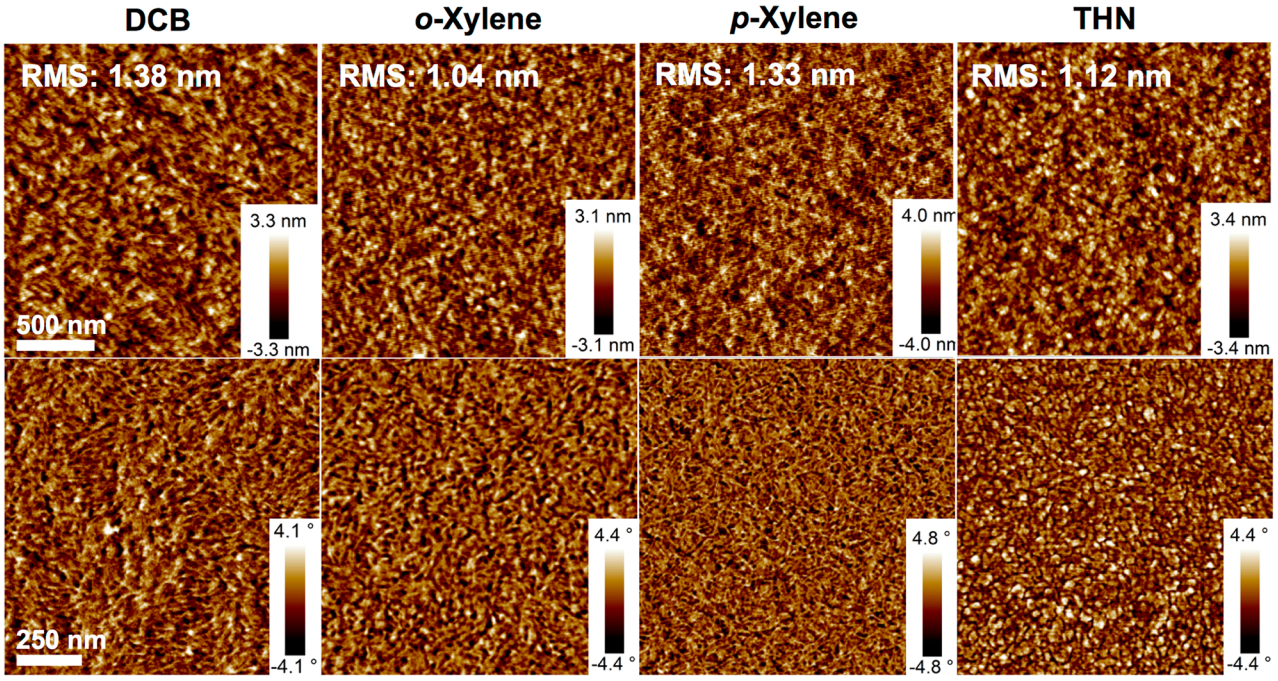

Figure 4. Tapping mode AFM height (top row) and phase (bottom row) images of **PDBTz** recorded after annealing each film at 150 °C for 30 min followed by rapid cooling to room temperature.

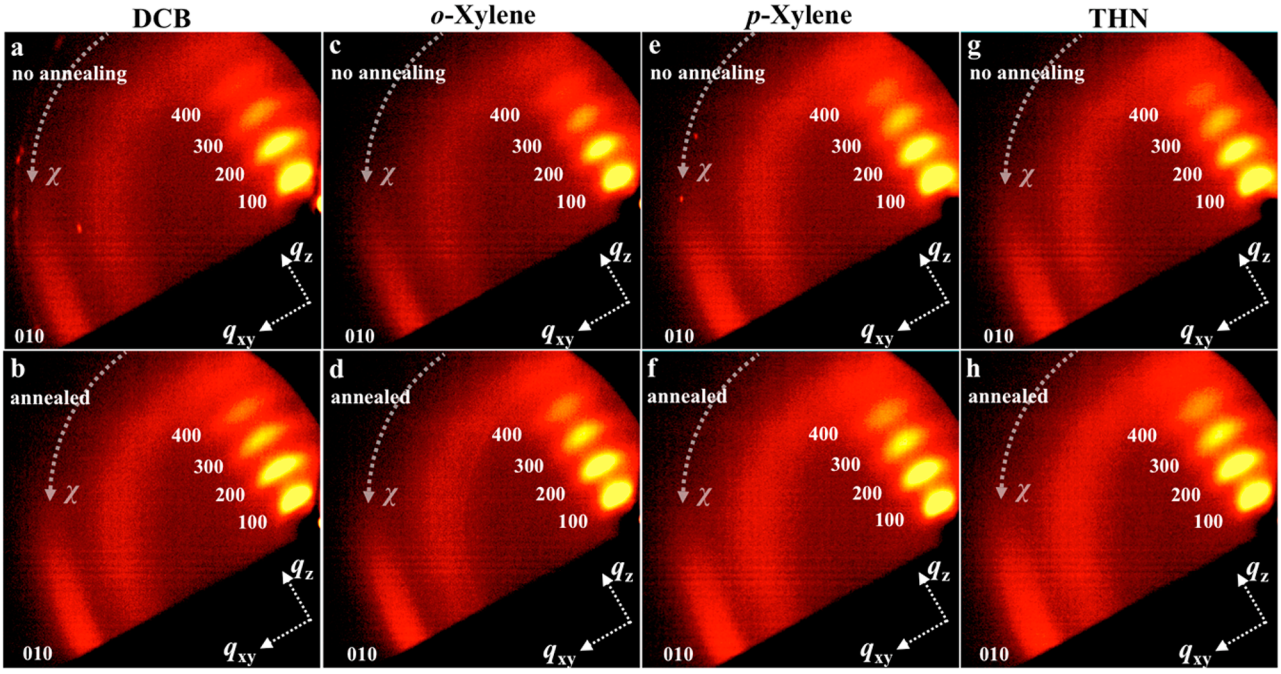

Figure 5. 2D-GIWAXS area detector images of PDBTz films cast from (a, b) DCB; (c, d) *o*-xylene; (e, f) *p*-xylene; and (g, h) THN solutions, respectively. Top row, as-spun films; bottom row, samples after annealing at 150 °C for 30 min followed by rapid cooling to room temperature.

electron injection, and taking into account the electron affinity of **PDBTz** (in the range of −3.8 to −3.9 eV), calcium (work function, φ = 2.9 eV)[51] and ethoxylated polyethylenimine (PEIE) doped silver (φ = 3.7 eV)[52] were selected as source and drain electrodes in TCBG and BCTG devices, respectively (Figure 2d). TCBG and BCTG OFETs were initially fabricated based on spin-coated **PDBTz**/DCB solutions (5 mg mL^{-1}). The results are listed in Table 4. TCBG OFETs making use of divinyltetramethylsiloxane-bis(benzocyclobutene) (BCB)[17,51] as the dielectric layer to minimize electron traps exhibited ideal n-channel *I*−*V* transfer characteristics, with average and maximum electron field-effect mobility values (μ_e) of 0.17 and 0.26 cm^2 V^{-1} s^{-1}, respectively, and a current on/off ratio ($I_{ON/OFF}$) greater than 1 × 10^5. Comparable electron-transport performance was determined for **PDBTz**-based BCTG OFETs with CYTOP/Al_2O_3 as dielectric and encapsulation bilayers. BCTG devices were characterized based on a 10 V source-drain voltage (V_{SD}) and a gate voltage (V_G) in a range of 0 to 16 V, revealing the feasibility of using **PDBTz** for high-performance devices under relatively low operating voltages. Notably, the

DOI: 10.1021/acs.chemmater.5b00173
Chem. Mater. 2015, 27, 2928−2937

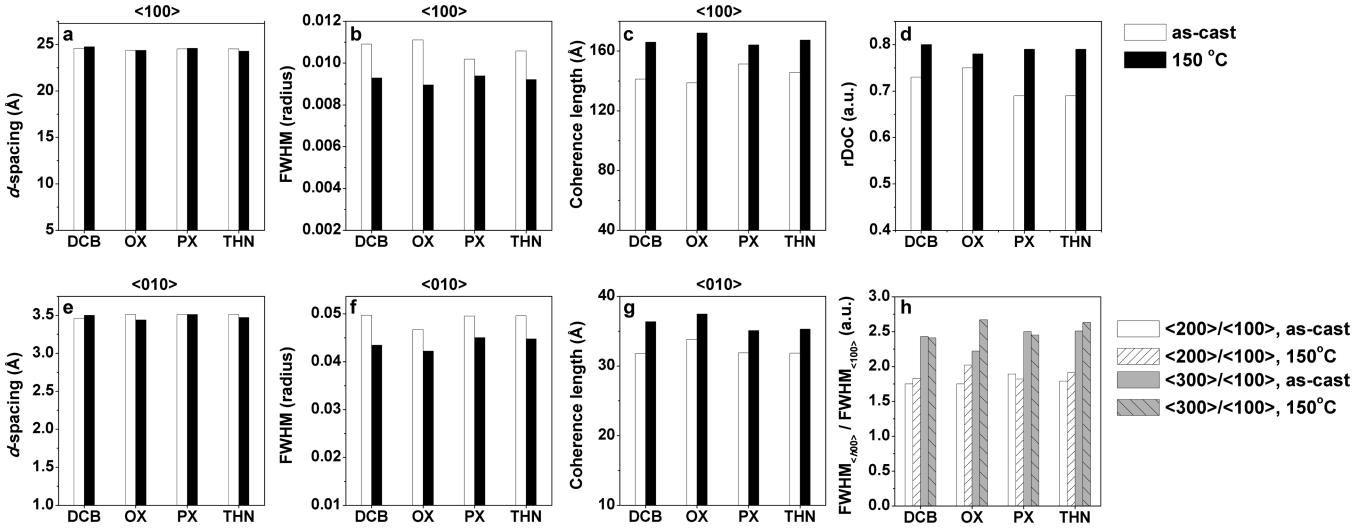

Figure 6. (a, e) *d*-spacing, (b, f) fwhm, and (c, g) coherence length for PDBTz cast from DCB, *o*-xylene (OX), *p*-xylene (PX), and tetrahydronaphthalene (THN) solutions, respectively, along the ⟨100⟩ and ⟨010⟩ peaks. (d) The relative degree of crystallinity (rDoC). Hollow bars, as cast films; black bars, films after 150 °C/30 min anneal. (h) Relative FWHMs of ⟨200⟩ and ⟨300⟩ to those of ⟨100⟩: $fwhm_{\langle 200\rangle}/fwhm_{\langle 100\rangle}$ and $fwhm_{\langle 300\rangle}/fwhm_{\langle 100\rangle}$ for as cast films (bars with no oblique line) and films after thermal annealing at 150 °C for 30 min (bars with oblique lines).

Table 5. Hermans' Orientation Function of ⟨100⟩ and ⟨010⟩ Peaks in PDBTz Films Cast from DCB, *o*-Xylene, *p*-Xylene, and THN, before and after Annealing

	RT[a]						150 °C[b]					
	⟨100⟩			⟨010⟩			⟨100⟩			⟨010⟩		
solvent	S[c]	χ_{max}[d]	$\Delta\chi_{fwhm}$[e]	S	χ_{max}	$\Delta\chi_{fwhm}$	S	χ_{max}	$\Delta\chi_{fwhm}$	S	χ_{max}	$\Delta\chi_{fwhm}$
DCB	0.85	1.8	12.3	0.66	4.5	21.3	0.83	1.9	11.7	0.62	3.5	23.1
o-xylene	0.88	1.9	9.7	0.76	3.8	19.7	0.90	1.1	7.6	0.77	4.4	19.2
p-xylene	0.87	2.8	10.9	0.81	4.6	17.0	0.89	1.4	8.4	0.79	4.0	19.0
THN	0.87	2.1	10.9	0.72	4.0	23.9	0.90	1.7	9.3	0.73	4.0	19.4

[a]**PDBTz** films as-spun from four solutions. [b]**PDBTz** films were thermally annealed at 150 °C for 30 min. [c]Hermans' orientation function. [d]The azimuthal angle at which X-ray scattering intensity reaches the maximum. [e]Absolute values of χ distribution corresponding to full width at half-maximum of peak intensity.

PDBTz devices exhibited similar performance to those prepared with poly(NDI2OD-T2) (0.1 $cm^2\ V^{-1}\ s^{-1}$), a benchmark electron-transport polymeric semiconductor, based on our previous study.[52] Both **PDBTz** device architectures exhibited excellent n-channel transistor behavior with low (4−8 V) threshold voltages (V_{th}) and negligible hysteresis (Figure 3b,f). The device performance was determined after thermal annealing at 150 °C. To explore **PDBTz** air stability, devices encapsulated by a CYTOP layer (Supporting Information) were stored at 25 °C and 55−70% RH, and were characterized periodically over 4 months. No appreciable changes were observed in $I_{ON/OFF}$ and only a small decrease in μ_e was observed over this period (Figure 3d, h). The ambient stability correlates with the low polymer frontier energy levels. Further enhancement of device stability against O_2 and H_2O is expected through inorganic/organic multilayer encapsulation.[53]

PDBTz possesses similar solubility in nonhalogenated *o*-xylene, *p*-xylene, and THN, as in DCB (vide supra). **PDBTz** OFET devices were also fabricated by spin-coating polymer solutions in *o*-xylene (5 mg mL^{-1}), *p*-xylene (4 mg mL^{-1}), and THN (5 mg mL^{-1}) to evaluate the impact of solution-processing from nonhalogenated vs halogenated solvents. As shown in Table 4, **PDBTz** electron-transport performance in BGTC devices was comparable in devices fabricated from all four solvents, with an average μ_e of 0.18 $cm^2\ V^{-1}\ s^{-1}$. A maximum value of μ_e (0.3 $cm^2\ V^{-1}\ s^{-1}$) was obtained in devices prepared from THN and *p*-xylene. **PDBTz**-based BCTG transistors fabricated from solutions in xylenes and THN exhibited μ_e (0.08 $cm^2\ V^{-1}\ s^{-1}$) relatively lower but close to that found for DCB (0.15 $cm^2\ V^{-1}\ s^{-1}$, in Table 4).

2.5. Thin Film Morphology and Microstructure. The surface morphologies of **PDBTz** films that were prepared by spin-casting from the four solutions onto BCB-modified Si substrates were characterized using tapping-mode atomic force microscopy (AFM). All of the films exhibited similar nanostructured morphologies with similar grain sizes of 30−60 nm and surface roughness of 1.04−1.38 nm, as shown in Figure 4. This suggests comparable contact between spin-coated films and the source-drain electrodes of TCBG OFETs.

The polymer films were investigated further by two-dimensional grazing incidence wide-angle X-ray scattering (2D-GIWAXS) to explore the relationship between film microstructure and electron-transport performance. Films were prepared from drop-cast **PDBTz** solutions in DCB, *o*-xylene, *p*-xylene, and THN onto Si substrates (300 nm SiO_2 dielectric on heavily p-doped Si) that had been functionalized with cross-linked BCB. X-ray scattering patterns, before and after thermal annealing at 150 °C, were similar for each sample, regardless of solvent, as shown in Figure 5. All of the films exhibited well-defined <*h*00> diffraction patterns along the q_z

DOI: 10.1021/acs.chemmater.5b00173
Chem. Mater. 2015, 27, 2928−2937

(out-of-plane) axis that is attributed to a highly ordered lamellar *d*-spacing structure between polymer chains that are segregated by 5-DH chains. In addition the films exhibited ⟨010⟩ peaks along the q_{xy} (in-plane) axis arising from $\pi-\pi$ stacking of **PDBTz** backbones. The spacing distances (Figure 6a, e), full-width at half-maximum (fwhm, Figure 6b, f), coherence length (mean size of ordered crystalline domains, Figure 6c, g), and relative degrees of crystallinity[15] (rDoC, Figure 6d) indicated by the ⟨100⟩ and ⟨010⟩ peaks are similar for **PDBTz** films from all four solutions both before and after annealing. In light of the length of a heptadecyl chain in an all-trans conformation (ca. 17.5 Å), the **PDBTz** lamellar *d*-spacing (24−25 Å) suggests that the side chains are interdigitated within the crystalline lattice.

The **PDBTz** ⟨100⟩ and ⟨010⟩ patterns exhibit highly anisotropic distributions along with the azimuthal angle, χ, as seen in Figure 5. This was quantitatively evaluated by Herman's orientation function (*S*, the calculation details are provided in the Supporting Information).[54] Results of this analysis are shown in Table 5. The four **PDBTz** films exhibited essentially identical *S* values that approached 0.9 for the ⟨100⟩ diffraction, which is regarded as a high value for a polymer system and is indicative of a high degree of alignment parallel to χ_{max}; on the other hand, χ_{max} for ⟨100⟩ is close to zero. These results quantitatively demonstrate that all four **PDBTz** films have average lattice planes oriented normal to the q_{xy} axis, which corresponds to an edge-on orientation, as shown in Scheme S1 in the Supporting Information. The $\Delta\chi_{FWMH}$ term refers to the full width at half-maximum of peak intensity along the χ axis. All four films display a value of $\Delta\chi_{FWMH}$ in a range of 9 to 13° for the ⟨100⟩ diffraction. Such a narrow distribution further confirms a high degree of orientation along χ_{max}. A similar phenomenon is observed for the ⟨010⟩ pattern: the four samples have an *S* value of approximately 0.8 at $\chi_{max} \approx 86°$. These results are also consistent with a highly aligned edge-on orientation for the average lattice planes, which mirrors the ⟨100⟩ analysis. In summary, all four **PDBTz** films exhibit a highly edge-on aligned orientation regardless of casting solvents.

The fwhm values for the ⟨200⟩ and ⟨300⟩ diffractions relative to that of the ⟨100⟩ diffraction (i.e., $fwhm_{\langle 200\rangle}/fwhm_{\langle 100\rangle}$ and $fwhm_{\langle 300\rangle}/fwhm_{\langle 100\rangle}$) underwent no obvious change upon annealing (Figure 6h), which demonstrates identical enhancement in the lattice cumulative order.[55] After annealing, all PDBTz films exhibited a reduction in fwhm and corresponding improvement in coherence length for both ⟨100⟩ and ⟨010⟩ patterns (Figure 6b, f and c, g), together with a 3−10% increase in rDoC, which correlate well with the observed increase in electron mobility upon annealing. In consideration of the subtle increase in orientation distribution within all four PDBTz films after thermal annealing, as shown by changes in *S* and $\Delta\chi_{FWMH}$ (Table 5), annealing primarily impacts PDBTz ordering and grain size, while crystallite growth likely proceeds equally along each orientation distribution direction. The microstructure and morphology analyses demonstrate that the processing solvents have similar effects on the morphology, molecular ordering, orientation, and rDoC of PDBTz films, in good accord with very similar electron-transport properties for the respective samples.

2.6. Comparison of PDBTz with PDQT. Several groups have reported the copolymerization of bithiophene-containing monomers and TDPP to afford poly(diketopyrrolopyrrole-quaterthiophene), PDQT,[35−37] whose chemical structure is shown in Figure 1d. Electrochemical studies of PDQT reveal reversible oxidation, and hole-transport properties are observed in OFETs prepared from this material. In contrast, **PDBTz**, where the bithiophene segment of each PDQT repeat unit is replaced by bithiazole, displays reversible electrochemical reduction and electron-transport behavior. This shift from hole transport for PDQT to electron transport for **PDBTz** clearly demonstrates a significant impact for bithiazole to instill electron-transport characteristics.

For a side-by-side comparison of these two polymers, **PDBTz** was applied to BCBG transistors with Au (φ = 5.1−5.5 eV) as source-drain electrodes, which have the same electrode-injection condition to PDQT based device. The results exhibited a 0.2−0.3 $cm^2\ V^{-1}\ s^{-1}$ of μ_e similar to those shown in TCBG and BCTG transistor configurations. A weak hole mobility (μ_h, on the order of $1 \times 10^{-3}\ cm^2\ V^{-1}\ s^{-1}$) was observed because of the close φ of Au to HOMO of **PDBTz**. This much greater μ_e than μ_h suggests that the bithiazole-based counterpart favors electron transport.

Density functional theory (DFT) calculations using tuned-ωB97X/cc-pVDZ were utilized to first explore the torsional potentials of **PDBTz** and PDQT subunits; the results were compared to reference single-point SCS-MP2 calculations (Figure 1a, see the Supporting Information for details).[56−58] Tuned-ωB97X calculations were also carried out for the monomer through tetramer of **PDBTz** and PDQT. The calculations indicate that within one **PDBTz** repeat unit, the bithiazole segment adopts a trans coplanar conformation with a dihedral angle (φ) of 180° between the two thiazole rings (Figure 1a). This contrasts with the bithiophene moiety within one PDQT repeat unit, in which the two rings are twisted at an angle of 155° (Figure 1a). Expectedly, replacing bithiophene with bithiazole stabilizes both the LUMO and HOMO levels of **PDBTz** by about 0.2−0.3 eV compared to PDQT (Figure 1b). Interestingly, as shown in Figure 1c, both the LUMO and HOMO wave functions are delocalized along the **PDBTz** backbone.

3. CONCLUSION

An electron-transport polymeric semiconductor, **PDBTz**, was prepared upon copolymerization of the electron-deficient bithiazole with dithienyldiketopyrrolopyrrole. **PDBTz** has a low optical bandgap (1.33 eV) and high electron affinity (−3.7 to −3.9 eV). **PDBTz**-based thin-film OFETs exhibited an electron mobility reaching 0.3 $cm^2\ V^{-1}\ s^{-1}$ with $I_{ON/OFF}$ greater than 1×10^5. No substantial performance changes were observed in $I_{ON/OFF}$ and a small decrease in μ_e was noted upon storing **PDBTz** OFETs encapsulated by CYTOP at 25 °C and 55−70% RH over 4 months. Incorporation of 5-DH side chains instilled **PDBTz** with good solubility in nonhalogenated xylenes and THN, in comparison to halogenated DCB. **PDBTz** films cast from these four solvents displayed similar morphologies (ordering and texture) and field-effect electron mobility. The results demonstrate the feasibility for developing high-performance electron-transport materials that are compatible with more environmentally benign process options. DFT calculations demonstrated that the incorporation of bithiazole induces a more planar geometry and lowers both the LUMO and HOMO energy levels compared to bithiophene, a typical electron-rich building block used to develop electron-transporting polymeric semiconductors.

Many current electron-transport and ambipolar polymeric semiconductors are based upon copolymerization of bithio-

DOI: 10.1021/acs.chemmater.5b00173
Chem. Mater. 2015, 27, 2928−2937

phene with electron acceptors, such as naphthalenedicarboximide, perylenedicarboximide, or isoindigo derivatives.[9,16,59−61] In this study, bithiazole has been shown as a promising building block for the next generation of electron-transport polymeric semiconductors with enhanced mobility and stability.

■ ASSOCIATED CONTENT

Supporting Information

The synthetic details of preparing monomers and polymers, characterization methods, OFET fabrications, computational details, Schemes S1 and S2, Table S1, and Figures S1−S11. This material is available free of charge via the Internet at http://pubs.acs.org.

■ AUTHOR INFORMATION

Corresponding Author

*E-mail: ereichmanis@chbe.gatech.edu.

Notes

The authors declare no competing financial interest.

■ ACKNOWLEDGMENTS

The authors gratefully acknowledge the contributions of Professor Alejandro Briseno and Ben Cherniawski of the Department of Polymer Science and Engineering at the University of Massachusetts Amherst (high-temperature GPC characterization) and of Professor John R. Reynolds and Kin Lo of the School of Chemistry and Biochemistry and the Georgia Tech Polymer Network at the Georgia Institute of Technology (CV and DPV characterization). This research was funded in part by the National Science Foundation (DMR-1207284), the Georgia Institute of Technology, and the Center for Organic Photonics and Electronics (COPE) Fellowship at Georgia Tech, as well as by the King Abdullah University of Science and Technology. 2D-GIXS measurements were carried out by Linda Sauer at the Characterization Facility, University of Minnesota, which receives partial support from NSF through the MRSEC program.

■ REFERENCES

(1) Baeg, K.-J.; Caironi, M.; Noh, Y.-Y. *Adv. Mater.* **2013**, *25*, 4210.
(2) Usta, H.; Facchetti, A.; Marks, T. J. *Acc. Chem. Res.* **2011**, *44*, 501.
(3) Russ, B.; Robb, M. J.; Brunetti, F. G.; Miller, P. L.; Perry, E. E.; Patel, S. N.; Ho, V.; Chang, W. B.; Urban, J. J.; Chabinyc, M. L.; Hawker, C. J.; Segalman, R. A. *Adv. Mater.* **2014**, *26*, 3473.
(4) Beaujuge, P. M.; Frechet, J. M. J. *J. Am. Chem. Soc.* **2011**, *133*, 20009.
(5) Zhou, E. J.; Cong, J. Z.; Wei, Q. S.; Tajima, K.; Yang, C. H.; Hashimoto, K. *Angew. Chem., Int. Ed.* **2011**, *50*, 2799.
(6) Schubert, M.; Dolfen, D.; Frisch, J.; Roland, S.; Steyrleuthner, R.; Stiller, B.; Chen, Z. H.; Scherf, U.; Koch, N.; Facchetti, A.; Neher, D. *Adv. Energy Mater.* **2012**, *2*, 369.
(7) Anthony, J. E.; Facchetti, A.; Heeney, M.; Marder, S. R.; Zhan, X. W. *Adv. Mater.* **2010**, *22*, 3876.
(8) Heidenhain, S. B.; Sakamoto, Y.; Suzuki, T.; Miura, A.; Fujikawa, H.; Mori, T.; Tokito, S.; Taga, Y. *J. Am. Chem. Soc.* **2000**, *122*, 10240.
(9) Yan, H.; Chen, Z. H.; Zheng, Y.; Newman, C.; Quinn, J. R.; Dotz, F.; Kastler, M.; Facchetti, A. *Nature* **2009**, *457*, 679.
(10) Zhang, Y.; Kim, C.; Lin, J.; Nguyen, T. Q. *Adv. Funct. Mater.* **2012**, *22*, 97.
(11) Kang, I.; Yun, H. J.; Chung, D. S.; Kwon, S. K.; Kim, Y. H. *J. Am. Chem. Soc.* **2013**, *135*, 14896.
(12) Tseng, H. R.; Phan, H.; Luo, C.; Wang, M.; Perez, L. A.; Patel, S. N.; Ying, L.; Kramer, E. J.; Nguyen, T. Q.; Bazan, G. C.; Heeger, A. J. *Adv. Mater.* **2014**, *26*, 2993.
(13) Zhao, Y.; Guo, Y. L.; Liu, Y. Q. *Adv. Mater.* **2013**, *25*, 5372.
(14) Lei, T.; Xia, X.; Wang, J.-Y.; Liu, C.-J.; Pei, J. *J. Am. Chem. Soc.* **2014**, *136*, 2135.
(15) Steyrleuthner, R.; Di Pietro, R.; Collins, B. A.; Polzer, F.; Himmelberger, S.; Schubert, M.; Chen, Z.; Zhang, S.; Salleo, A.; Ade, H.; Facchetti, A.; Neher, D. *J. Am. Chem. Soc.* **2014**, *136*, 4245.
(16) Li, H. Y.; Kim, F. S.; Ren, G. Q.; Jenekhe, S. A. *J. Am. Chem. Soc.* **2013**, *135*, 14920.
(17) Chua, L. L.; Zaumseil, J.; Chang, J. F.; Ou, E. C. W.; Ho, P. K. H.; Sirringhaus, H.; Friend, R. H. *Nature* **2005**, *434*, 194.
(18) Wang, C. L.; Dong, H. L.; Hu, W. P.; Liu, Y. Q.; Zhu, D. B. *Chem. Rev.* **2012**, *112*, 2208.
(19) Chen, H. Y.; Hou, J. H.; Zhang, S. Q.; Liang, Y. Y.; Yang, G. W.; Yang, Y.; Yu, L. P.; Wu, Y.; Li, G. *Nat. Photonics* **2009**, *3*, 649.
(20) Fu, B. Y.; Baltazar, J.; Hu, Z. K.; Chien, A. T.; Kumar, S.; Henderson, C. L.; Collard, D. M.; Reichmanis, E. *Chem. Mater.* **2012**, *24*, 4123.
(21) Coropceanu, V.; Cornil, J.; da Silva, D. A.; Olivier, Y.; Silbey, R.; Bredas, J. L. *Chem. Rev.* **2007**, *107*, 926.
(22) Lin, Y. Z.; Fan, H. J.; Li, Y. F.; Zhan, X. W. *Adv. Mater. (Weinheim, Ger.)* **2012**, *24*, 3087.
(23) Liu, Y.; Dong, H. L.; Jiang, S. D.; Zhao, G. Y.; Shi, Q. Q.; Tan, J. H.; Jiang, L.; Hu, W. P.; Zhan, X. W. *Chem. Mater.* **2013**, *25*, 2649.
(24) Mamada, M.; Nishida, J. I.; Kumaki, D.; Tokito, S.; Yamashita, Y. *Chem. Mater.* **2007**, *19*, 5404.
(25) Wolf, M. O.; Wrighton, M. S. *Chem. Mater.* **1994**, *6*, 1526.
(26) Yamamoto, T.; Suganuma, H.; Maruyama, T.; Inoue, T.; Muramatsu, Y.; Arai, M.; Komarudin, D.; Ooba, N.; Tomaru, S.; Sasaki, S.; Kubota, K. *Chem. Mater.* **1997**, *9*, 1217.
(27) Jung, I. H.; Jung, Y. K.; Lee, J.; Park, J. H.; Woo, H. Y.; Lee, J. I.; Chu, H. Y.; Shim, H. K. *J. Polym. Sci., Polym. Chem.* **2008**, *46*, 7148.
(28) Tao, T.; Peng, Y. X.; Huang, W.; You, X. Z. *J. Org. Chem.* **2013**, *78*, 2472.
(29) Johansson, M. P.; Olsen, J. *J. Chem. Theory Comput.* **2008**, *4*, 1460.
(30) Breitung, E. M.; Shu, C. F.; McMahon, R. J. *J. Am. Chem. Soc.* **2000**, *122*, 1154.
(31) Bak, B.; Christensen, D.; Hansen-Nygaard, L.; Rastrup-Andersen, J. *J. Mol. Spectrosc.* **1962**, *9*, 222.
(32) Usta, H.; Sheets, W. C.; Denti, M.; Generali, G.; Capelli, R.; Lu, S.; Yu, X.; Muccini, M.; Facchetti, A. *Chem. Mater.* **2014**, *26*, 6542.
(33) Ando, S.; Nishida, J. I.; Tada, H.; Inoue, Y.; Tokito, S.; Yamashita, Y. *J. Am. Chem. Soc.* **2005**, *127*, 5336.
(34) Balan, B.; Vijayakumar, C.; Saeki, A.; Koizumi, Y.; Seki, S. *Macromolecules* **2012**, *45*, 2709.
(35) Li, Y. N.; Sonar, P.; Singh, S. P.; Soh, M. S.; van Meurs, M.; Tan, J. *J. Am. Chem. Soc.* **2011**, *133*, 2198.
(36) Zhang, X. R.; Richter, L. J.; DeLongchamp, D. M.; Kline, R. J.; Hammond, M. R.; McCulloch, I.; Heeney, M.; Ashraf, R. S.; Smith, J. N.; Anthopoulos, T. D.; Schroeder, B.; Geerts, Y. H.; Fischer, D. A.; Toney, M. F. *J. Am. Chem. Soc.* **2011**, *133*, 15073.
(37) Liu, F.; Wang, C.; Baral, J. K.; Zhang, L.; Watkins, J. J.; Briseno, A. L.; Russell, T. P. *J. Am. Chem. Soc.* **2013**, *135*, 19248.
(38) Fu, B. Y.; Baltazar, J.; Sankar, A. R.; Chu, P. H.; Zhang, S. Y.; Collard, D. M.; Reichmanis, E. *Adv. Funct. Mater.* **2014**, *24*, 3734.
(39) Chueh, C. C.; Yao, K.; Yip, H. L.; Chang, C. Y.; Xu, Y. X.; Chen, K. S.; Li, C. Z.; Liu, P.; Huang, F.; Chen, Y. W.; Chenb, W. C.; Jen, A. K. Y. *Energy Environ. Sci.* **2013**, *6*, 3241.
(40) Lee, W. Y.; Giri, G.; Diao, Y.; Tassone, C. J.; Matthews, J. R.; Sorensen, M. L.; Mannsfeld, S. C. B.; Chen, W. C.; Fong, H. H.; Tok, J. B. H.; Toney, M. F.; He, M. Q.; Bao, Z. A. *Adv. Funct. Mater.* **2014**, *24*, 3524.
(41) Chen, Y.; Zhang, S. Q.; Wu, Y.; Hou, J. H. *Adv. Mater.* **2014**, *26*, 2744.
(42) Yun, H.-J.; Lee, G. B.; Chung, D. S.; Kim, Y.-H.; Kwon, S.-K. *Adv. Mater.* **2014**, *26*, 6612.
(43) Lemaire, M.; Hassan, J.; Lavenot, L.; Gozzi, C. *Tetrahedron Lett.* **1999**, *40*, 857.
(44) Chang, M.; Choi, D.; Fu, B. Y.; Reichmanis, E. *ACS Nano* **2013**, *7*, 5402.

DOI: 10.1021/acs.chemmater.5b00173
Chem. Mater. 2015, 27, 2928−2937

(45) Graham, K. R.; Wieruszewski, P. M.; Stalder, R.; Hartel, M. J.; Mei, J. G.; So, F.; Reynolds, J. R. *Adv. Funct. Mater.* **2012**, *22*, 4801.
(46) Spano, F. C.; Silva, C. *Annu. Rev. Phys. Chem.* **2014**, *65*, 477.
(47) Hellmann, C.; Paquin, F.; Treat, N. D.; Bruno, A.; Reynolds, L. X.; Haque, S. A.; Stavrinou, P. N.; Silva, C.; Stingelin, N. *Adv. Mater.* **2013**, *25*, 4906.
(48) Cardona, C. M.; Li, W.; Kaifer, A. E.; Stockdale, D.; Bazan, G. C. *Adv. Mater.* **2011**, *23*, 2367.
(49) Stalder, R.; Mei, J. G.; Subbiah, J.; Grand, C.; Estrada, L. A.; So, F.; Reynolds, J. R. *Macromolecules* **2011**, *44*, 6303.
(50) Bredas, J.-L. *Mater. Horiz.* **2014**, *1*, 17.
(51) Tiwari, S. P.; Zhang, X. H.; Potscavage, W. J.; Kippelen, B. *J. Appl. Phys.* **2009**, *106*, 054504.
(52) Zhou, Y. H.; Fuentes-Hernandez, C.; Shim, J.; Meyer, J.; Giordano, A. J.; Li, H.; Winget, P.; Papadopoulos, T.; Cheun, H.; Kim, J.; Fenoll, M.; Dindar, A.; Haske, W.; Najafabadi, E.; Khan, T. M.; Sojoudi, H.; Barlow, S.; Graham, S.; Bredas, J. L.; Marder, S. R.; Kahn, A.; Kippelen, B. *Science* **2012**, *336*, 327.
(53) Kim, N.; Potscavage, W. J.; Domercq, B.; Kippelen, B.; Graham, S. *Appl. Phys. Lett.* **2009**, *94*, 163308.
(54) Perez, L. A.; Zalar, P.; Ying, L.; Schmidt, K.; Toney, M. F.; Nguyen, T. Q.; Bazan, G. C.; Kramer, E. J. *Macromolecules* **2014**, *47*, 1403.
(55) Rivnay, J.; Steyrleuthner, R.; Jimison, L. H.; Casadei, A.; Chen, Z. H.; Toney, M. F.; Facchetti, A.; Neher, D.; Salleo, A. *Macromolecules* **2011**, *44*, 5246.
(56) Dunning, T. H. *J. Chem. Phys.* **1989**, *90*, 1007.
(57) Woon, D. E.; Dunning, T. H. *J. Chem. Phys.* **1993**, *98*, 1358.
(58) Chai, J. D.; Head-Gordon, M. *J. Chem. Phys.* **2008**, *128*, 084106.
(59) Chen, Z. H.; Zheng, Y.; Yan, H.; Facchetti, A. *J. Am. Chem. Soc.* **2009**, *131*, 8.
(60) Li, W.; Roelofs, W. S. C.; Turbiez, M.; Wienk, M. M.; Janssen, R. A. J. *Adv. Mater.* **2014**, *26*, 3304.
(61) Sun, B.; Hong, W.; Yan, Z. Q.; Aziz, H.; Li, Y. N. *Adv. Mater.* **2014**, *26*, 2636.

DOI: 10.1021/acs.chemmater.5b00173
Chem. Mater. 2015, 27, 2928−2937